CLEG

Cai Liu, Ning Liu, and Yang Liu

JLU — TABLE OF CONTENTS

Adaptive prediction filtering in t-x-y domain for random noise attenuation using regularized nonstationary autoregression

Yang Liu, Ning Liu, and Cai Liu

ABSTRACT

Many natural phenomena, including geologic events and geophysical data, are fundamentally nonstationary. They may exhibit stationarity on a short timescale but eventually alter their behavior in time and space. We propose a 2D t-x adaptive prediction filter (APF) and further extend this to a 3D t-x-y version for random noise attenuation based on regularized nonstationary autoregression (RNA). Instead of using patching, a popular method for handling nonstationarity, we obtain smoothly nonstationary APF coefficients by solving a global regularized least-squares problem. We use shaping regularization to control the smoothness of the coefficients of APF. 3D space-noncausal t-x-y APF uses neighboring traces around the target traces in the 3D seismic cube to predict noise-free signal, so it provides more accurate prediction results than the 2D version. In comparison with other denoising methods, such as frequency-space deconvolution, time-space prediction filter, and frequency-space RNA, we test the feasibility of our method in reducing seismic random noise on three synthetic datasets. Results of applying the proposed method to seismic field data demonstrate that nonstationary t-x-y APF is effective in practice.

INTRODUCTION

Attenuation of noise is a persistent problem in seismic exploration. Random noise can come from various sources. Although stacking can at least partly suppress random noise in prestack data, residual random noise after stacking will decrease the accuracy of the final data interpretation. In recent years, several authors have developed effective methods of eliminating random noise. For example, Ristau and Moon (2001) compared several adaptive filters, which they applied in an attempt to reduce random noise in geophysical data. Karsli et al. (2006) applied complex-trace analysis to seismic data for random-noise suppression, recommending it for low-fold seismic data. Some transform methods were also used to deal with seismic random noise, e.g., the discrete cosine transform (Lu and Liu, 2007), the curvelet transform (Neelamani et al., 2008), and the seislet transform (Fomel and Liu, 2010).

Seismic reflections are recorded according to special geometry and always appear lateral continuity, which is used to distinguish events from the background noise. If

events of interest are linear (lines in 2D data and planes in 3D data), one can predict linear events by using prediction techniques in the frequency-space domain or the time-space domain (Abma and Claerbout, 1995). The f-x prediction technique was introduced by Canales (1984) and further developed by Gulunay (1986), and is a standard industry method known as "FXDECON". Sacchi and Kuehl (2001) utilized the autoregressive-moving average (ARMA) structure of the signal to estimate f-x prediction-error filter (PEF) and the noise sequence. Liu et al. (2012) developed f-x regularized nonstationary autoregression (RNA) to attenuate random noise. Liu and Chen (2013) further extended 2D f-x RNA to 3D noncausal regularized nonstationary autoregression (NRNA) for random noise elimination.

The prediction process can be also achieved in t-x domain (Claerbout, 1992). Abma and Claerbout (1995) discussed f-x and t-x approaches to predict linear events from random noise. t-x prediction always passes less random noise than f-x prediction method because the f-x prediction technique, while dividing the prediction problem into separate problems for each frequency, produces a filter as long as the data series in time. However, seismic data are naturally nonstationary, and a standard t-x prediction filter can only be used to process stationary data (Claerbout, 1992). Patching is a common method to handle nonstationarity (Claerbout, 2010), although it occasionally fails in the assumption of piecewise constant dips. Crawley et al. (1999) proposed smoothly nonstationary prediction-error filters (PEFs) with "micropatches" and radial smoothing, which typically produces better results than the rectangular patching approach. Fomel (2002) developed a plane-wave destruction (PWD) filter (Claerbout, 1992) as an alternative to t-x PEF and applied a PWD operator to represent nonstationary. However, PWD method depends on the assumption of a small number of smoothly variable seismic dips. When background random noise is strong, the dip estimation is a difficult problem. Sacchi and Naghizadeh (2009) proposed an algorithm to compute time and space variant prediction filters for noise attenuation, which is implemented by a recursive scheme where the filter is continuously adapted to predict the signal.

In this paper, we propose a t-x adaptive prediction filter (APF) to preserve nonstationary signal and attenuate random noise. The key idea is the use of shaping regularization (Fomel, 2007) to constrain the time and space smoothness of filter coefficients in the corresponding ill-posed autoregression problem. The structure of space-causal and space-noncausal APF is also discussed. We test nonstationary characteristics of APF by using a 2D synthetic curved model, a 2D synthetic poststack model, and a 3D prestack French model. Results of applying the proposed method to the field example demonstrate that regularized APF can be effective in eliminating random noise.

THEORY

t-x adaptive prediction filtering using RNA

Consider a 2D prediction filter (general for stationary PF) with ten prediction coefficients $B_{i,j}$:

$$\begin{array}{ccc} \cdot & B_{-2,1} & B_{-2,2} \\ \cdot & B_{-1,1} & B_{-1,2} \\ 1(t,x) & B_{0,1} & B_{0,2} \\ \cdot & B_{1,1} & B_{1,2} \\ \cdot & B_{2,1} & B_{2,2} \end{array} \tag{1}$$

where i is time shift, j is space shift, the vertical axis is time axis, and the horizontal axis is space axis. The output position is under the "$1(t,x)$" coefficient on the left side of filter and "$1(t,x)$" indicates time- and space-varying samples. The filter is noncausal along the time axis and causal along the space axis. More filter structures will be discussed later. The PF has the different coefficients from PEF, which includes causal time prediction coefficients.

To obtain stationary PF coefficients, one can solve the over-determined least-squares problem

$$\tilde{B}_{i,j} = \arg\min_{B_{i,j}} \|S(t,x) - \sum_{j=1}^{N} \sum_{i=-M}^{M} B_{i,j} S_{i,j}(t,x)\|_2^2 \,, \tag{2}$$

where $S_{i,j}(t,x)$ represents the translation of linear events $S(t,x)$ in both time and space directions with time shift i and space shift j. The choice of the filter size depends on the maximum dip of the plane waves in the data and the number of dips. For nonlinear events, cutting data into overlapping windows (patching) is a common method to handle nonstationarity (Claerbout, 2010), although it occasionally fails in the presence of variable dips.

For nonstationary situations, we can also assume local linearization of the data. For estimating APF coefficients, nonstationary autoregression allows the coefficients $B_{i,j}$ to change with both t and x. The new adaptive filter can be designed as

$$\begin{array}{ccc} \cdot & B_{-2,1}(t,x) & B_{-2,2}(t,x) \\ \cdot & B_{-1,1}(t,x) & B_{-1,2}(t,x) \\ 1(t,x) & B_{0,1}(t,x) & B_{0,2}(t,x) \\ \cdot & B_{1,1}(t,x) & B_{1,2}(t,x) \\ \cdot & B_{2,1}(t,x) & B_{2,2}(t,x) \end{array} \tag{3}$$

In the linear notation, prediction coefficients $B_{i,j}(t,x)$ can be obtained by solving

the under-determined least-squares problem

$$\tilde{B}_{i,j}(t,x) = \arg\min_{B_{i,j}(t,x)} \|S(t,x) - \sum_{j=1}^{N}\sum_{i=-M}^{M} B_{i,j}(t,x)S_{i,j}(t,x)\|_2^2 + \epsilon^2 \sum_{j=1}^{N}\sum_{i=-M}^{M} \|\mathbf{D}[B_{i,j}(t,x)]\|_2^2 \,, \quad (4)$$

where $\mathbf{D}$ is the regularization operator and ϵ is a scalar regularization parameter. This approach was described by Fomel (2009) as regularized nonstationary autoregression (RNA). Shaping regularization (Fomel, 2007) specified a shaping (smoothing) operator $\mathbf{R}$ instead of $\mathbf{D}$ and provided better numerical properties than Tikhonov's regularization (Tikhonov, 1963) in equation 4. The advantages of the shaping regularization include an intuitive selection of regularization parameters and fast iteration convergence. Coefficients $B_{i,j}(t,x)$ get constrained by regularization. The required parameters are the size and shape of the filter, $B_{i,j}(t,x)$, and the smoothing radius for shaping regularization. The size of APF controls the range and the number of the predicted dips. Larger filter parameters, N and M, are able to predict more accurate dips, however, the APFs with the large filter size pass more random noise and add more computational cost. As the smoothing radius of the APF increases, the APF removes not only more random noise but also some structural details. The APF is able to be extended to the adaptive PEF (APEF), which shows a expected representation of nonstationary signal and is fit for seismic data interpolation (Liu and Fomel, 2011) and random noise attenuation (Liu and Liu, 2011). However, the structure of APEF is different from that of APF, which excludes the causal time prediction coefficients and forces only lateral predictions. Meanwhile, in this paper, we use a two-step method that estimates APF coefficients by solving an under-determined problem and calculates noise-free signal. The proposed method is different from the two-step APEF denoising including APEF estimation for signal and noise plus signal and noise separation by solving a least-square system as shown in Liu and Liu (2011).

3D space-noncausal adaptive prediction filtering

Equation 2 and 4 show space-forward prediction equations, which are similar as the causal prediction filtering equations in f-x domain (Gulunay, 2000). Furthermore, t-x prediction filter also includes time-noncausal coefficients. In the case of both space-forward and space-backward prediction equations (space-noncausal prediction filter), equation 4 can be written (Spitz, 1991; Naghizadeh and Sacchi, 2009; Liu et al., 2012; Liu and Chen, 2013) with the results averaged:

$$\tilde{B}_{i,j}(t,x) = \arg\min_{B_{i,j}(t,x)} \|S(t,x) - \sum_{j=-N,j\neq 0}^{N}\sum_{i=-M}^{M} B_{i,j}(t,x)S_{i,j}(t,x)\|_2^2 + \epsilon^2 \sum_{j=-N,j\neq 0}^{N}\sum_{i=-M}^{M} \|\mathbf{R}[B_{i,j}(t,x)]\|_2^2 \,, \quad (5)$$

Equation 5 shows that one sample in t-x domain can be predicted by the samples in adjacent traces with weight coefficients $B_{i,j}(t,x)$, which is time- and space-varying. The equation assumes that the seismic data only consist of plane waves $\sum_{j=-N,j\neq 0}^{N}\sum_{i=-M}^{M} B_{i,j}(t,x)S_{i,j}(t,x)$ and random noise that corresponds to a least-squares error.

Figure 1a shows a 2D space-causal APF structure, which is time-noncausal filter. White grids stand for prediction samples and the dark-grey grid is the output (or target) position, while light-grey grids are unused samples. The filter size of the space-causal APF is $N \times (2M+1)$. Meanwhile, space-noncausal APF (Figure 1b) has a symmetric structure along time and space axes. The filter size of the space-noncausal APF is $2N \times (2M+1)$. The 3D t-x-y APF also has space-causal or space-noncausal structure, Figure 2 shows the noncausal one. In a 3D seismic datacube, the plane events can be predicted along two different spatial directions. A 2D t-x APF will have difficulty preserving accurate plane waves because it only uses the information in x or y direction, however, a 3D t-x-y APF provides a more natural structure. t-x-y adaptive prediction filtering for random noise attenuation follows two steps:

1. Estimating 3D space-noncausal APF coefficients $\tilde{B}_{i,j,k}(t,x,y)$ by solving the regularized least-squares problem (equation 4 or 5 in 2D):

$$\tilde{B}_{i,j,k}(t,x,y) = \arg\min_{B_{i,j,k}(t,x,y)} \|S(t,x,y) - \sum_{k=-L,k\neq 0}^{L}\sum_{j=-N,j\neq 0}^{N}\sum_{i=-M}^{M} B_{i,j,k}(t,x,y)S_{i,j,k}(t,x,y)\|_2^2 + \epsilon^2 \sum_{k=-L,k\neq 0}^{L}\sum_{j=-N,j\neq 0}^{N}\sum_{i=-M}^{M} \|\mathbf{R}[B_{i,j,k}(t,x,y)]\|_2^2 \,, \tag{6}$$

2. Calculating noise-free signal $\tilde{S}(t,x,y)$ according to

$$\tilde{S}(t,x,y) = \sum_{k=-L,k\neq 0}^{L}\sum_{j=-N,j\neq 0}^{N}\sum_{i=-M}^{M} \tilde{B}_{i,j,k}(t,x,y)S_{i,j,k}(t,x,y) \,, \tag{7}$$

SYNTHETIC DATA TEST

2D curved model

We start with a synthetic example (Figure 3a) created by Raymond Abma, which was originally used for testing nonstationary interpolation (Liu and Fomel, 2011). The number of time samples is 401 and the number of space samples is 240. Figure 3b is the data with uniformly-distributed random noise added. We compare t-x APF with f-x deconvolution (Gulunay, 1986), t-x PF (Abma and Claerbout, 1995), and f-x

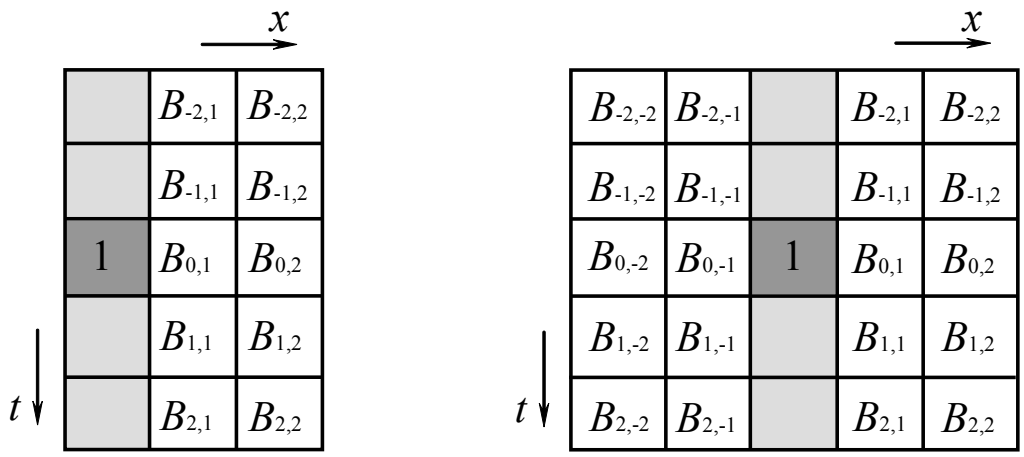

Figure 1: Schematic illustration of a 2D *t*-*x* APF. A space-causal filter (a) and a space-noncausal filter (b). txyapf/. causal2d,noncausal2d

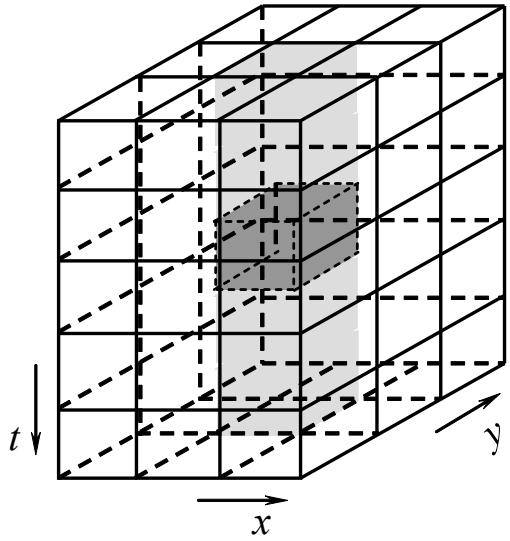

Figure 2: Schematic illustration of a 3D *t*-*x*-*y* space-noncausal APF. txyapf/. noncausal3d

RNA (Liu et al., 2012) and test their ability for random noise attenuation. Figure 4 shows the denoised results by using stationary methods. Both the f-x deconvolution and the t-x PF fail in handling nonstationary curved events. The data was divided into 5 patches with 40% overlap along space axis. f-x deconvolution eliminates both signal and noise (Figure 4a and 4b) and creates some artificial events with weak energy, which are parallel with the curved event. t-x PF preserves signal better and introduces artifacts fewer than f-x deconvolution (Figure 4c), but the difference (Figure 4d) between Figure 3b and 4c also shows obvious signal.

Another approach is to apply nonstationary filters. The denoised results by using f-x RNA and t-x APF are shown in Figure 5a and 5c, respectively. The filter length of f-x RNA is 8 and it has a 10-sample (frequency) and 20-sample (space) smoothing radius. f-x RNA (Figure 5a) has a better result than stationary methods, e.g., f-x deconvolution (Figure 4a) and t-x PF (Figure 4c), however, there is still signal trend in the noise section (Figure 4b) and artificial events appear that are similar to those from f-x deconvolution. For the t-x APF, the choice of the filter length in space is similar to that in f-x RNA. We tend to use a 12-sample filter in space, and the filter length in time for the t-x APF is selected to five samples. As the time-length of the t-x APF increases, the t-x APF passes more random noise. We use the shaping regularization with a 60-sample (time) and 20-sample (space) smoothing radius to constrain the APF coefficient space. The denoised result and removed noise are shown in Figure 5c and 5d, respectively. t-x APF also introduces a few artifacts, but the artifacts show a random-trend distribution (Figure 5c). Meanwhile, the t-x APF, shown in Figure 5d, preserves signal better than the f-x RNA.

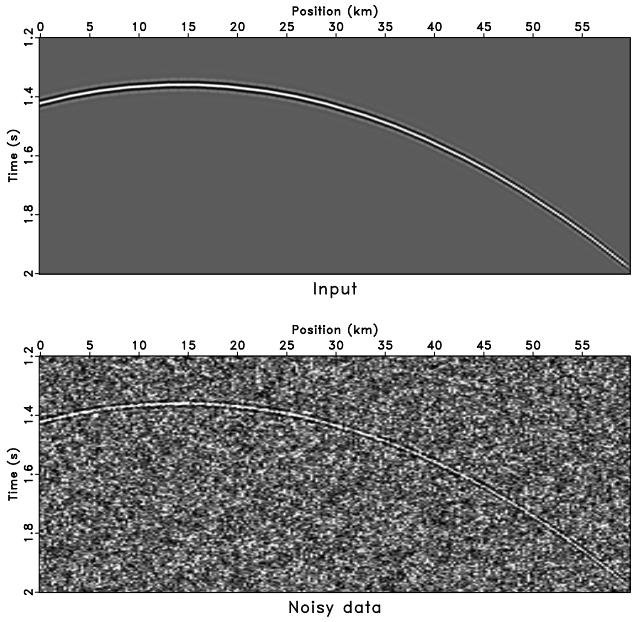

Figure 3: Curved model (a) and noisy data (b). txyapf/curve jcacov,noiz

For further discussion, we added extra spike noise to Figure 3b, the new noisy

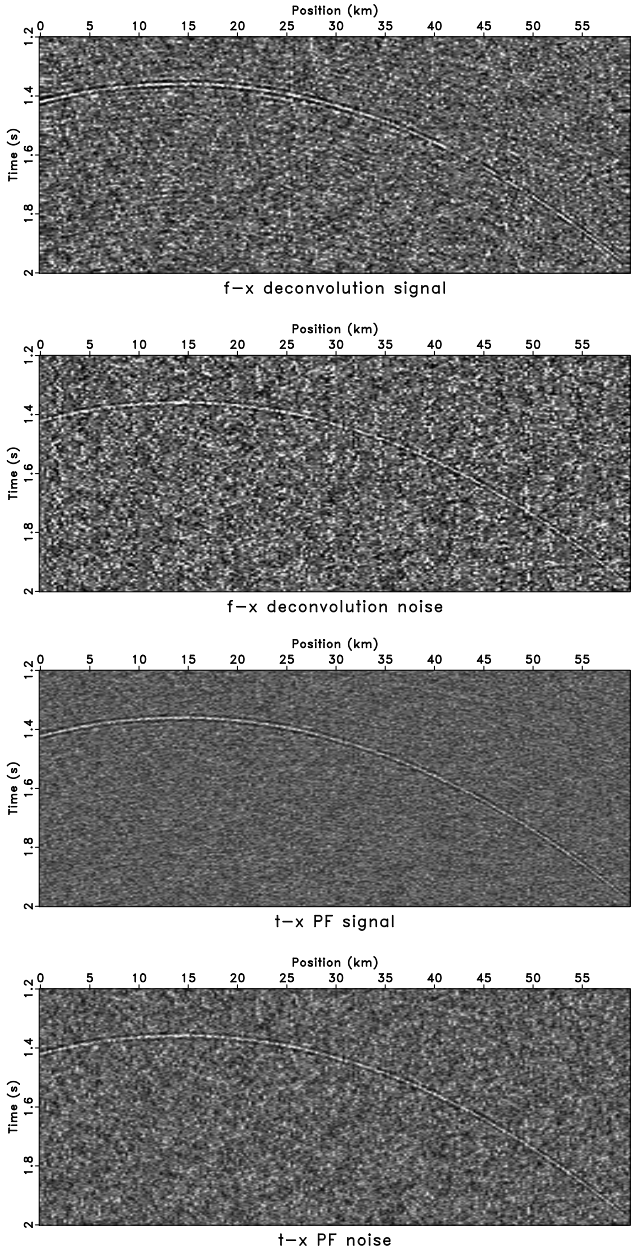

Figure 4: Comparison of stationary methods. The denoised result by f-x deconvolution (a), the noise removed by f-x deconvolution (b), the denoised result by t-x PF (c), and the noise removed by t-x PF (d). txyapf/curve fxpatch,fxdiff,txpatch,txdiff

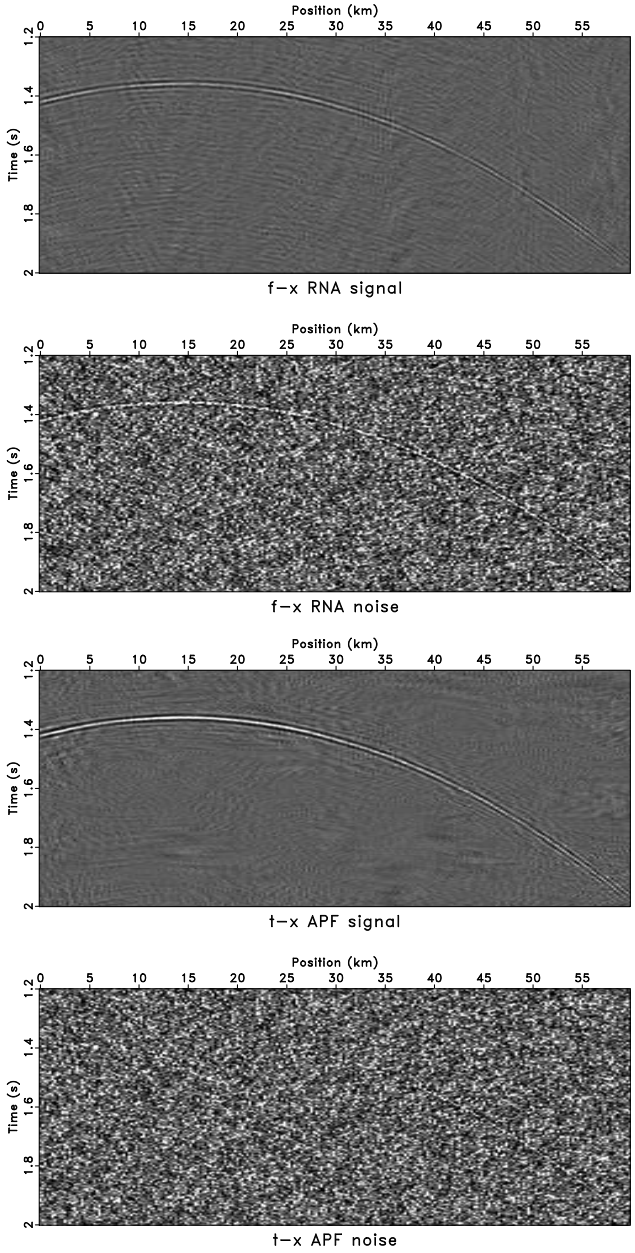

Figure 5: Comparison of nonstationary methods. The denoised result by f-x RNA (a), the noise removed by f-x RNA (b), the denoised result by t-x APF (c), and the noise removed by t-x APF (d). txyapf/curve fxrna,fxnoiz,aspred,asnoiz

model with a wiggle display is shown in Figure 6a. When comparing with the t-x PF with patching (Figure 6b) and the f-x RNA (Figure 6c), the t-x APF shows better signal-protection ability, however, the quality of the denoised result gets worse than Figure 5c because of the spikes (Figure 6d). Larger smoothing radius can reduce the artifacts at the cost of attenuating part of the signals.

2D poststack model

The second example is shown in Figure 7a. The input data are borrowed from Claerbout (2009): a synthetic seismic image containing dipping beds, an unconformity and a fault. Figure 7b shows the same image with Gaussian noise added. The challenge in this example is to account for both nonstationary and event truncations. Figure 8a shows the denoised result using the f-x RNA, which was implemented in each frequency slice. Note that the f-x RNA can eliminate part of noise, but the result shows some artificial events, which are parallel with the events. The difference (Figure 8b) between Figure 7b and Figure 8a also shows the corresponding artifacts. The denoised result and the noise removed using the t-x APF are shown in Figure 8c and Figure 8d, respectively. The APF has 10 (time) $\times$ 10 (space) coefficients for each sample and a 20-sample (time) $\times$ 20-sample (space) smoothing radius. The proposed method eliminates most of random noise and preserves the truncations well.

3D prestack French model

We created a 3D example by Kirchhoff modeling (Figure 9a), the corresponding velocity model is a slice out of the benchmark French model (French, 1974; Liu and Fomel, 2010). Three surfaces of Figure 9a illustrate the corresponding slices at time=0.6s, midpoint=1.0km, and half-offset=0.2km. Figure 9b is the noisy data. The challenge in this example is to account for multi-dimension, nonstationarity, and conflicting dips. For comparison, we use 3D f-x-y NRNA (Liu and Chen, 2013) to attenuate random noise (Figure 10a). The 3D NRNA method produces a reasonable result. In Figure 10b, 3D f-x-y NRNA shows a better ability of signal preservation than 2D version (Liu et al., 2012). However, 3D NRNA still produces artificial events parallel with curved events. We design a 3D t-x-y APF with 5 (time) $\times$ 4 (midpoint) $\times$ 4 (half offset) coefficients for each sample and 15-sample (time), 10-sample (midpoint), and 10-sample (half offset) smoothing radius to further handle the variability of event. Figure 10c and 10d show the denoised result and the difference between noisy data (Figure 9b) and the denoised result (Figure 10c) plotted at the same clip value, respectively. The proposed method succeeds in the sense that it is hard to distinguish the curved and conflicting events in the removed noise. Meanwhile, the 3D t-x-y APF has fewer artificial events, which are more visible for 3D f-x-y NRNA (Figure 10a).

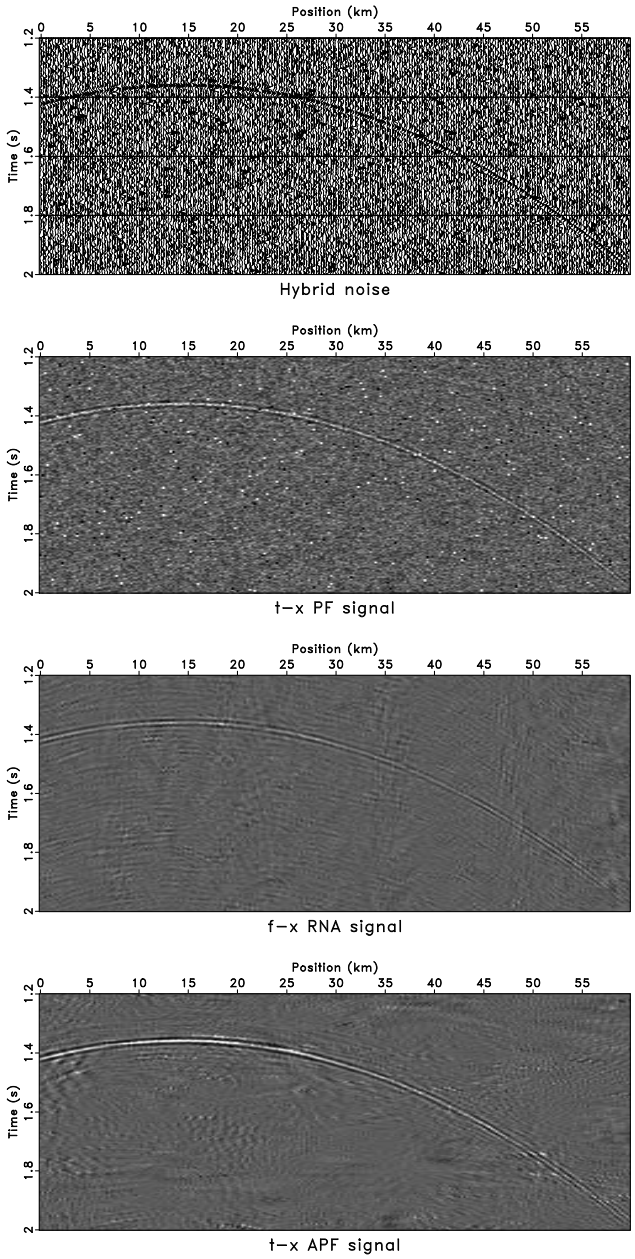

Figure 6: Tests of hybrid noise model by using different methods. Data with hybrid noise (a), *t-x* PF (b), *f-x* RNA (c), and *t-x* APF (d). txyapf/curve noiz1,txpatch1,fxrna1,aspred1

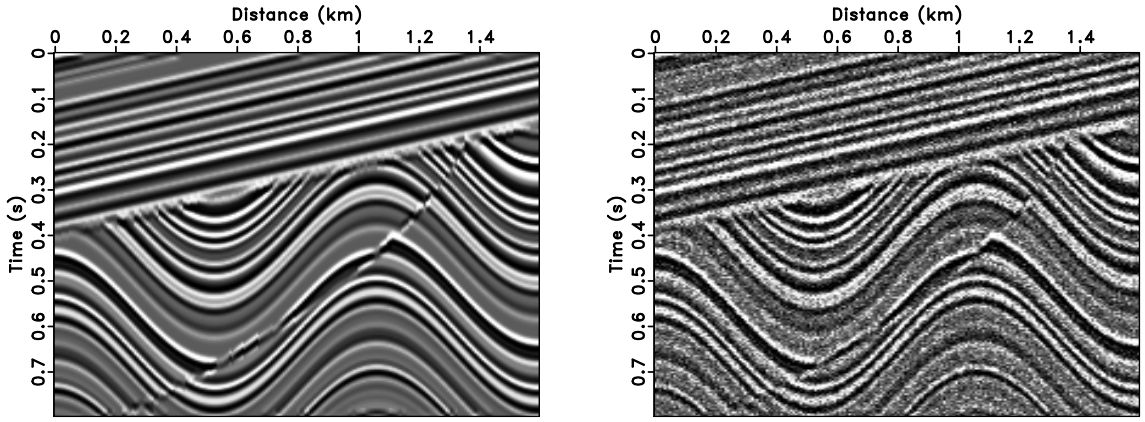

Figure 7: 2D poststack model (a) and noisy data (b). txyapf/sigmoid sigmoid,noise

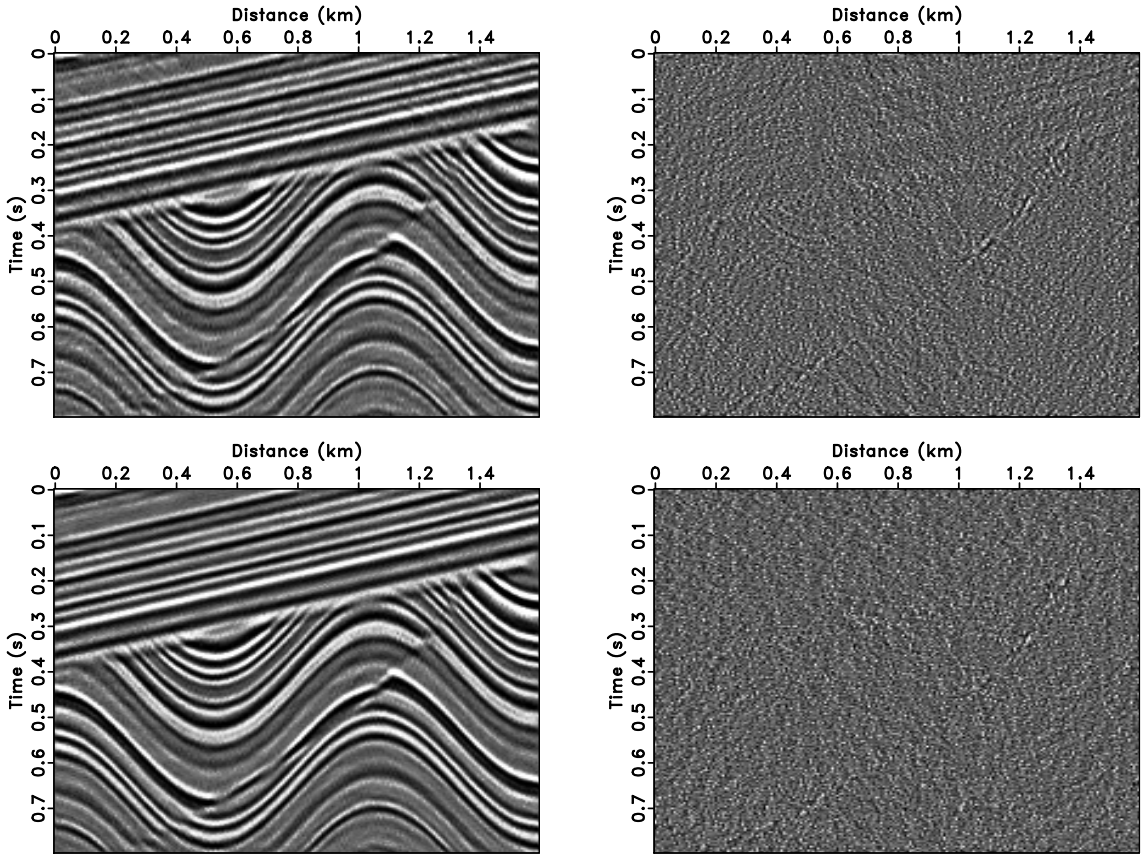

Figure 8: Comparison of nonstationary methods. The denoised result by f-x RNA (a), the noise removed by f-x RNA (b), the denoised result by t-x APF (c), and the noise removed by t-x APF (d). txyapf/sigmoid sfxrna,sfxnoiz,apfs,apfn

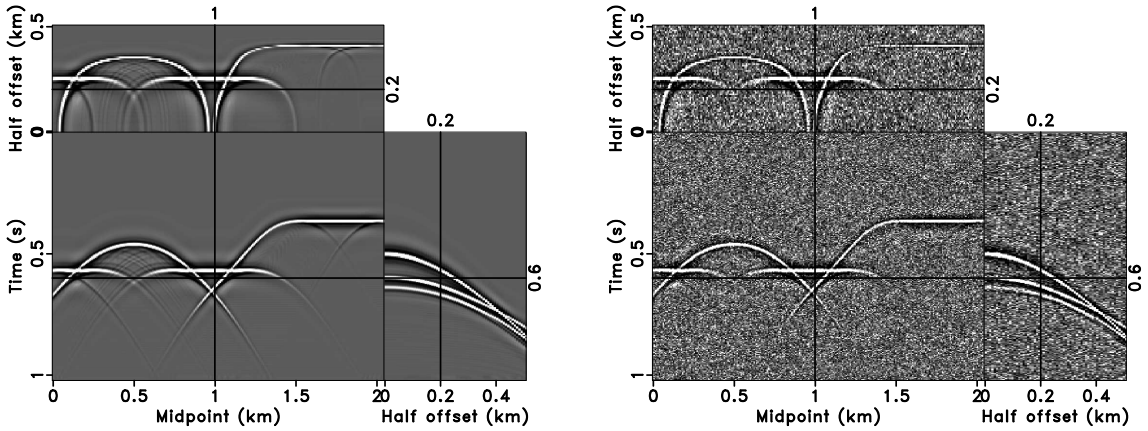

Figure 9: 3D synthetic data (a) and the corresponding noisy data (b). txyapf/french fdata,fnoise

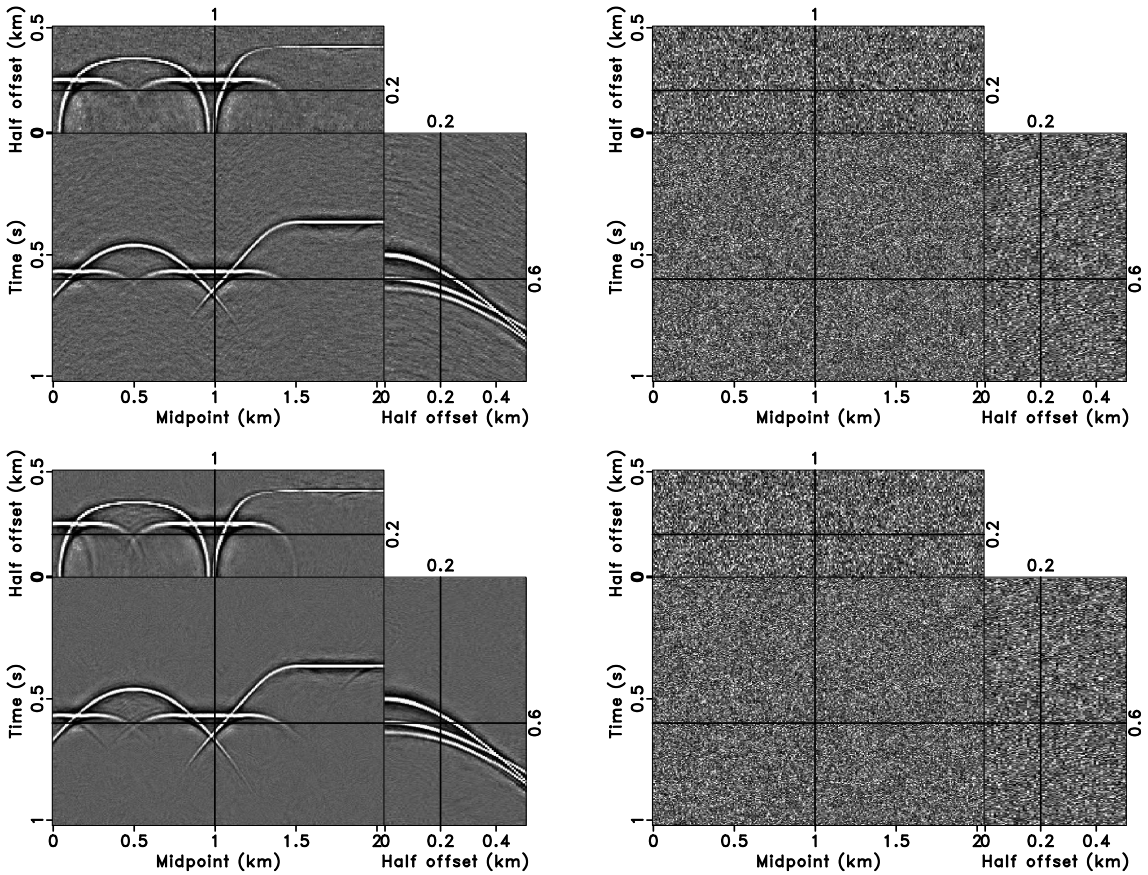

Figure 10: The denoised result by 3D f-x-y NRNA (a), the noise removed by 3D f-x-y NRNA (b), the denoised result by 3D t-x-y APF (c), and the noise removed by 3D t-x-y APF (d). txyapf/french tpre,diff3d,fpred3,ferr3

FIELD DATA TEST

For the field data test, we use a time-migrated seismic image from Liu and Chen (2013). The input is shown in Figure 11. The three sections in Figure 11 show the time slice at time position of 0.34 s (top section), X line section at Y space position of 7.62 km (bottom left section), and Y line section at X space position of 1.41 km (bottom right section). The datacube displays simple plane layers above 1.0 s and complex structure below 1.0 s. Noise is mainly strong random noise caused by the surface conditions in this area. For comparison, we apply f-x-y NRNA to remove the random noise. We use a total of 24 neighboring traces around each output trace after applying a Fourier transform along time axis. The denoised result is shown in Figure 12, which gives a much clearer lateral continuity than original field data. f-x-y NRNA improves the both shallow plane events and deep dipping events. Figure 14 shows the difference section, in which the processed data using f-x-y NRNA have been subtracted from the original data. Some horizontal events are shown in Figure 14, especially at locations from 0.3 s to 1.0 s in Y line section (bottom right section). Figure 13 shows that the proposed t-x-y APF method also produces reasonable result, where continuity of events and geology structure are enhanced, and there is little noise left. The t-x-y APF parameters correspond to 5 (time) $\times$ 4 (X) $\times$ 4 (Y) coefficients for each sample (M=2, N=2, and L=2 in Equation 6 and 7) and 20-sample (time), 10-sample (X), and 10-sample (Y) smoothing radius for regularization operator $\mathbf{R}$. After carefully comparing with the filtering result of 3D f-x-y NRNA (Figure 12), 3D t-x-y APF (Figure 13) can be seen to preserve more detailed structure because t-x-y APF has extra nonstationarity along time axis while f-x-y NRNA only consider nonstationarity along the two space axis. Splitting into windows can partly help f-x-y NRNA to improve the result, but it still cannot provide a naturally nonstationary domain. Comparing with Figure 14, the difference (Figure 15) between Figure 11 and Figure 13 shows no obvious horizontal events and random noise is more uniformly-distributed.

CONCLUSIONS

We have introduced a new approach to adaptive prediction filter (APF) for seismic random noise attenuation in t-x-y domain. Our approach uses regularized nonstationary autoregression (RNA) to handle time-space variation of nonstationary seismic data. These properties are useful for application such as random noise attenuation. The predicted signal provides a noise-free estimation of local plane events. Compared with the f-x-y NRNA method, t-x-y APF can capture more detailed signal and avoid most artifacts, which occur more in frequency domain methods. However, the f-x-y NRNA method uses fewer prediction coefficients (no time prediction) to save storage space and can be applied in parallel to different frequency slices. Therefore, f-x-y NRNA is appropriate for mild complex structure and fast computation while t-x-y APF is more appropriate for very complex structures. Experiments with synthetic examples and field data tests show that the proposed filters are able to depict variations

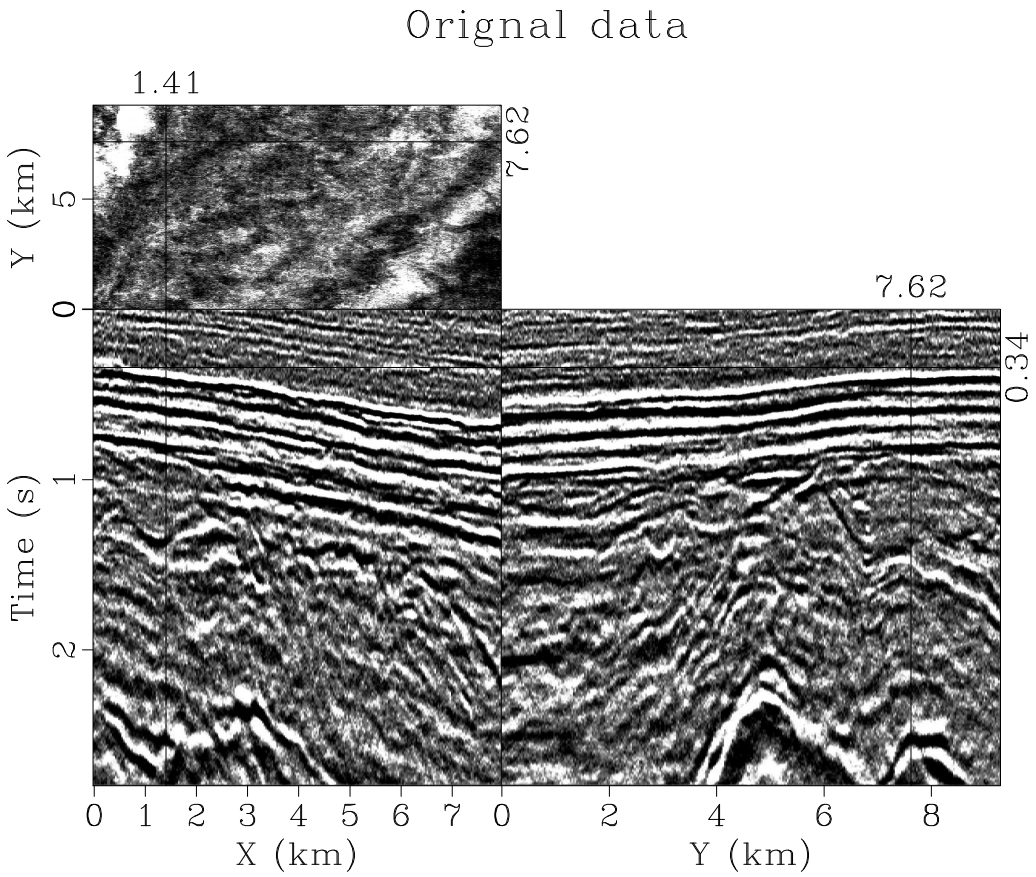

Figure 11: 3D field data. txyapf/real3d data

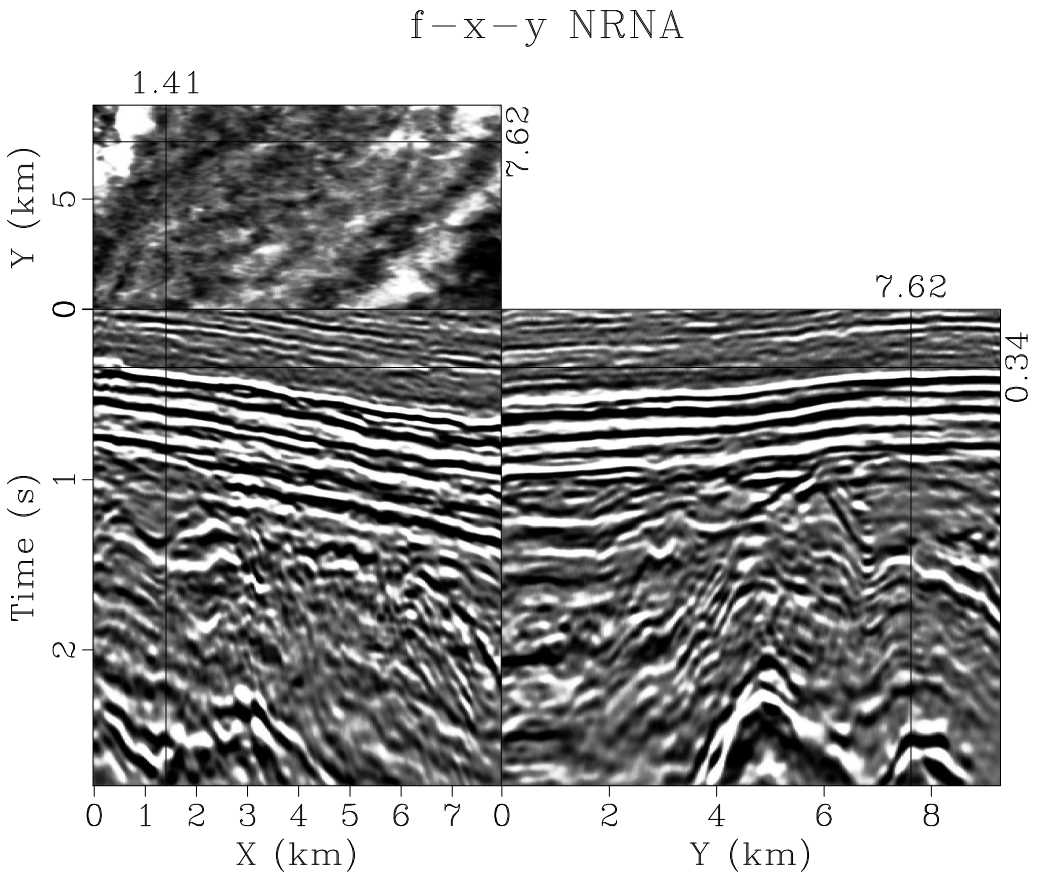

Figure 12: The denoised result by using 3D f-x-y NRNA. txyapf/real3d tpre1

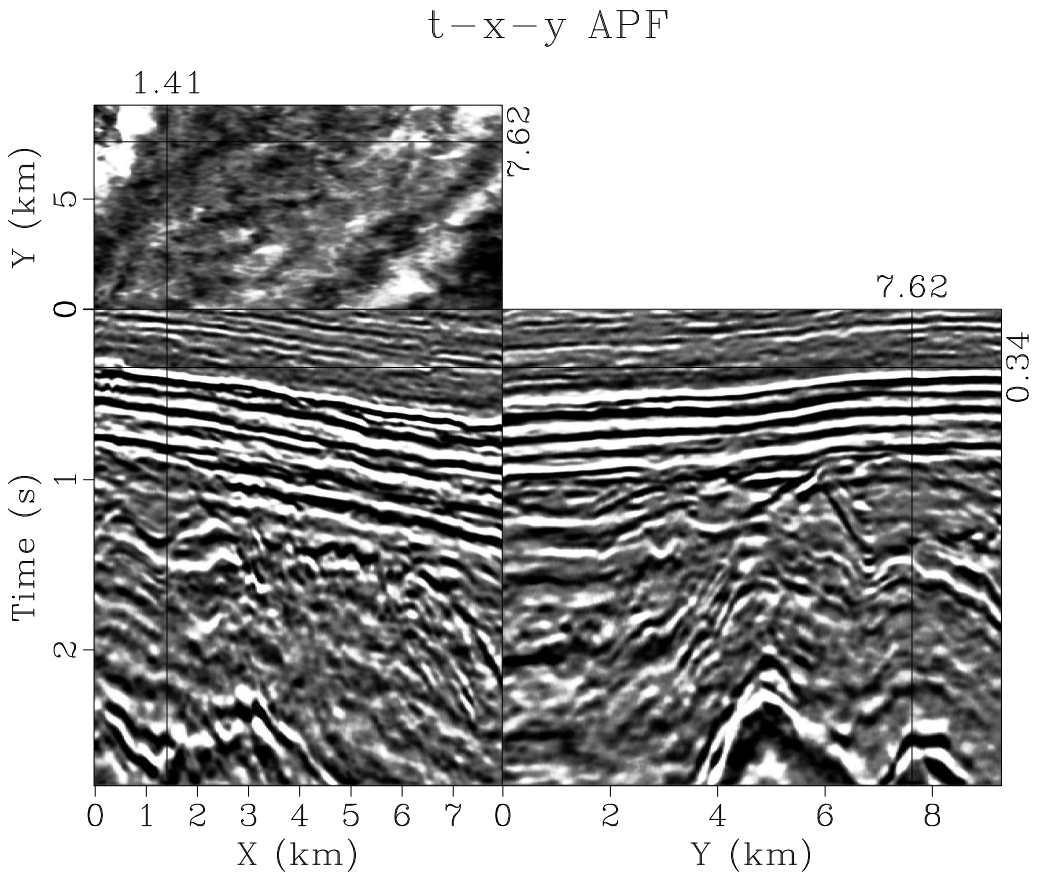

Figure 13: The denoised result by using 3D *t-x-y* APF. txyapf/real3d ppred3

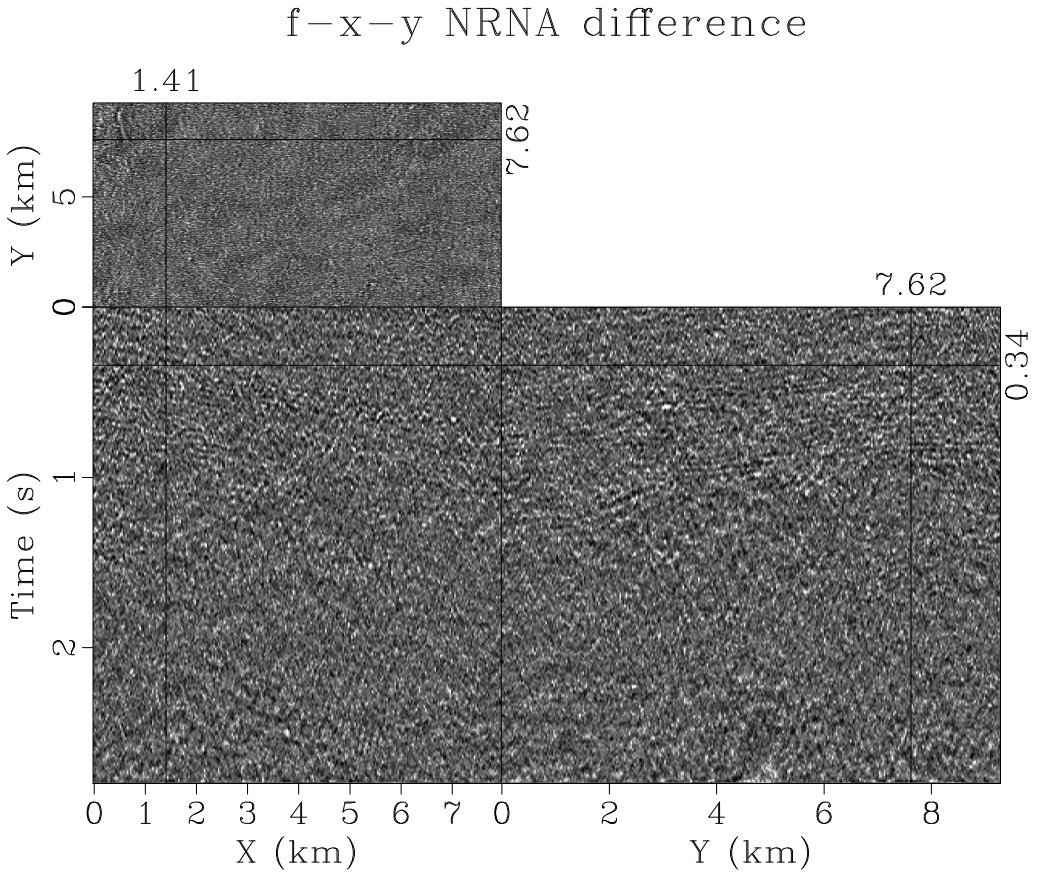

Figure 14: The difference between the noisy data (Figure 11) and the denoised result by using 3D *f*-*x*-*y* NRNA (Figure 12). txyapf/real3d diff3d

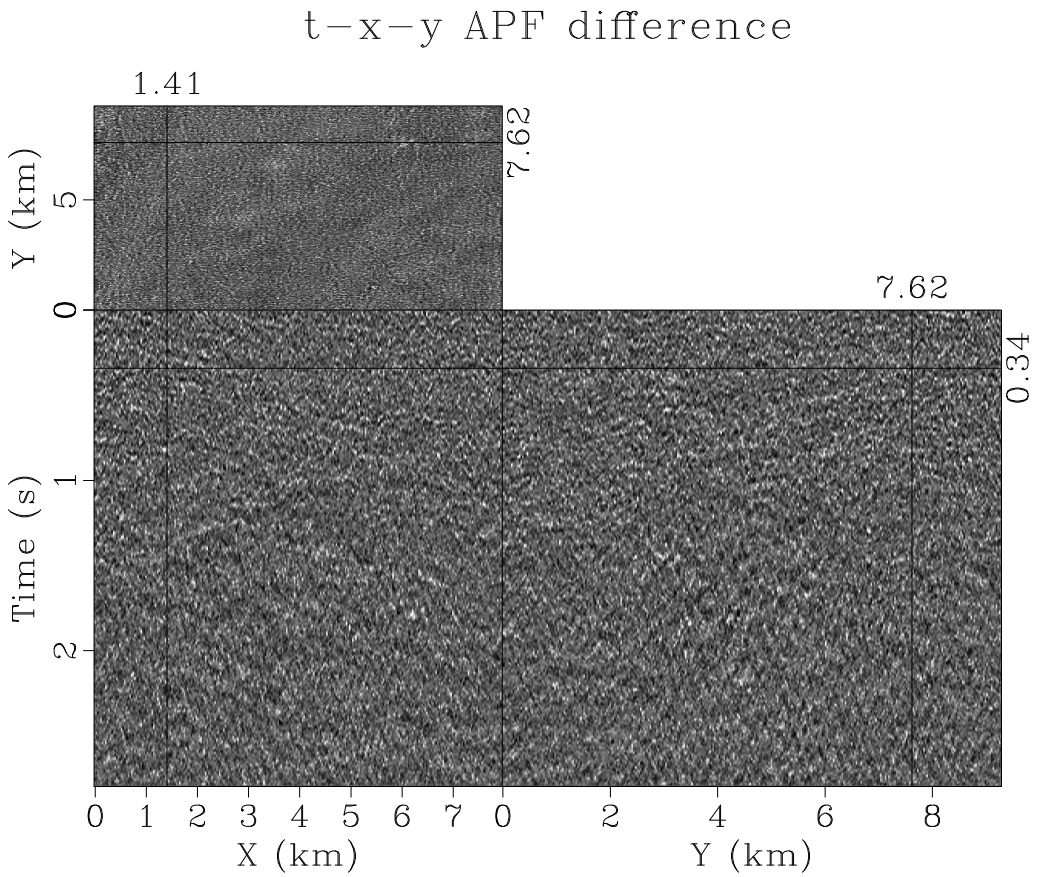

Figure 15: The difference between the noisy data (Figure 11) and the denoised result by using 3D *t-x-y* APF (Figure 13). txyapf/real3d diff3

in the nonstationary signal and provide a accurate estimation of complex wavefields even in the presence of strongly curved and conflicting events.

ACKNOWLEDGMENTS

We thank Jeffrey Shragge, Kris Innanen, and three anonymous reviewers for helpful suggestions, which improved the quality of the paper. This work is partly supported by National Natural Science Foundation of China (Grant No. 41274119, 41430322), 863 Program of China (Grant No. 2012AA09A2010), and 973 Program of China (Grant No. 2013CB429805). All results are reproducible in the Madagascar open-source software environment (Fomel et al., 2013).

REFERENCES

Abma, R., and J. Claerbout, 1995, Lateral prediction for noise attenuation by t-x and f-x techniques: Geophysics, **60**, 1887–1896.

Canales, L. L., 1984, Random noise reduction: 54th Annual International Meeting, SEG, Expanded Abstracts, Session: S10.1.

Claerbout, J. F., 1992, Earth Soundings Analysis: Processing Versus Inversion: Blackwell Scientific Publications.

———, 2009, Basic earth imaging: Stanford Exploration Project, `http://sepwww.stanford.edu/sep/prof/`.

———, 2010, Geophysical image estimation by example - Multidimensional autoregression: Stanford Exploration Project, http://sepwww.stanford.edu/sep/prof/.

Crawley, S., J. F. Claerbout, and R. Clapp, 1999, Interpolation with smoothly nonstationary prediction-error filters: 69th Annual International Meeting, SEG, Expanded Abstracts, 1154–1157.

Fomel, S., 2002, Applications of plane-wave destruction filters: Geophysics, **67**, 1946–1960.

———, 2007, Shaping regularization in geophysical-estimation problems: Geophysics, **72**, R29–R36.

———, 2009, Adaptive multiple subtraction using regularized nonstationary regression: Geophysics, **74**, V25–V33.

Fomel, S., and Y. Liu, 2010, Seislet transform and seislet frame: Geophysics, **75**, V25–V38.

Fomel, S., P. Sava, I. Vlad, Y. Liu, and V. Bashkardin, 2013, Madagascar: open-source software project for multidimensional data analysis and reproducible computational experiments: Journal of Open Research Software, **1**, e8.

French, W. S., 1974, Two-dimensional and three-dimensional migration of model-experiment reflection profiles: Geophysics, **39**, 265–277.

Gulunay, N., 1986, Fx decon and complex Wiener prediction filter: 56th Annual International Meeting, SEG, Expanded Abstracts, Session: POS2.10.

———, 2000, Noncausal spatial prediction filtering for random noise reduction on 3-D poststack data: Geophysics, **65**, 1641–1653.

Karsli, H., D. Dondurur, and G. Çifçi, 2006, Application of complex-trace analysis to seismic data for random-noise suppression and temporal resolution improvement: Geophysics, **71**, V79–V86.

Liu, G. C., and X. H. Chen, 2013, Noncausal f-x-y regularized nonstationary prediction filtering for random noise attenuation on 3D seismic data: Journal of Applied Geophysics, **93**, 60–66.

Liu, G. C., X. H. Chen, J. Du, and K. L. Wu, 2012, Random noise attenuation using f-x regularized nonstationary autoregression: Geophysics, **77**, V61–V69.

Liu, Y., and S. Fomel, 2010, OC-seislet: seislet transform construction with differential offset continuation: Geophysics, **75**, WB235–WB245.

———, 2011, Seismic data interpolation beyond aliasing using regularized nonstationary autoregression: Geophysics, **76**, V69–V77.

Liu, Y., and C. Liu, 2011, Nonstationary signal and noise separation using adaptive prediction-error filter: 81st Annual International Meeting, SEG, Expanded Abstracts, 3601–3606.

Lu, W., and J. Liu, 2007, Random noise suppression based on discrete cosine transform: 77th Annual International Meeting, SEG, Expanded Abstracts, 2668–2672.

Naghizadeh, M., and M. Sacchi, 2009, f-x adaptive seismic-trace interpolation: Geophysics, **74**, V9–V16.

Neelamani, R., A. I. Baumstein, D. G. Gillard, M. T. Hadidi, and W. I. Soroka, 2008, Coherent and random noise attenuation using the curvelet transform: The Leading Edge, **27**, 240–248.

Ristau, J. P., and W. M. Moon, 2001, Adaptive filtering of random noise in 2-D geophysical data: Geophysics, **66**, 342–349.

Sacchi, M., and H. Kuehl, 2001, ARMA formulation of FX prediction error filters and projection filters: Journal of Seismic Exploration, **9**, 185–197.

Sacchi, M., and M. Naghizadeh, 2009, Adaptive linear prediction filtering for random noise attenuation: 79th Annual International Meeting, SEG, Expanded Abstracts, 3347–3351.

Spitz, S., 1991, Seismic trace interpolation in the F-X domain: Geophysics, **56**, 785–794.

Tikhonov, A. N., 1963, Solution of Incorrectly Formulated Problems and the Regularization Method: Soviet Mathematics – Doklady.